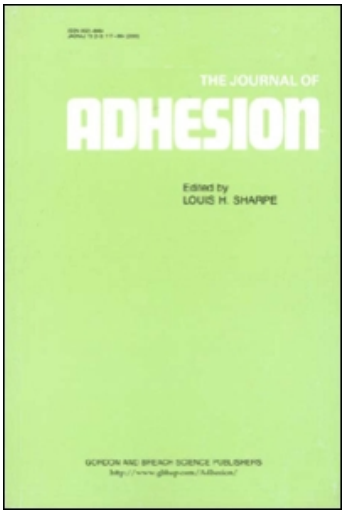

The Journal of Adhesion

Publication details, including instructions for authors and subscription information:
http://www.informaworld.com/smpp/title~content=t713453635

Removal of Particle Pairs from a Plane Surface

Goodarz Ahmadi[a]; Haifeng Zhang[a]; Ruijing Han[b]; Bernard Greenspan[b]
[a] Department of Mechanical and Aeronautical Engineering, Clarkson University, Potsdam, New York, USA [b] Elan (Dura) Pharmaceuticals, San Diego, California, USA

To cite this Article Ahmadi, Goodarz , Zhang, Haifeng , Han, Ruijing and Greenspan, Bernard(2005) 'Removal of Particle Pairs from a Plane Surface', The Journal of Adhesion, 81: 2, 189 — 212
To link to this Article: DOI: 10.1080/00218460590922002
URL: http://dx.doi.org/10.1080/00218460590922002

The Journal of Adhesion, 81:189–212, 2005

ISSN: 0021-8464 print/1545-5823 online
DOI: 10.1080/00218460590922002

Taylor & Francis
Taylor & Francis Group

Removal of Particle Pairs from a Plane Surface

Goodarz Ahmadi
Haifeng Zhang
Department of Mechanical and Aeronautical Engineering, Clarkson University, Potsdam, New York, USA

Ruijing Han
Bernard Greenspan
Elan (Dura) Pharmaceuticals, San Diego, California, USA

The removal of two attached particle pairs from a plane surface was studied. The computational fluid dynamics code FLUENT™ was used to evaluate the drag force and to simulate the flow field around the two attached spherical particles that are in contact with a plane subject to a shear flow. Critical shear rates for various vertically aligned particle-pair removal mechanisms from a plane surface are evaluated. The results show that rolling detachment is the dominant mechanism for removal of particle pairs from a plane surface, and the presence of fine surface roughness reduces the critical shear rate. It is also found that it is easier for a vertically aligned particle pair with the large particle on the top to be removed from the wall when compared with a pair with the large particle in contact with wall.

Keywords: Breaup; Detachment; Particle-pair adhesion; Particle-pair drag; pair removal

Received 1 April 2004; in final form 1 November 2004.

Various stages of this work were supported by Elan (Dura) Pharmaceuticals, Inc.; Environmental Protection Agency (EPA); and New York State Office of Science, Technology and Academic Research (NYSTAR) [through the Center for Advanced Materials Processing (CAMP) of Clarkson University]. The support of IBM through the donation of pSeries computational facilities to Clarkson University is also gratefully acknowledged.

Address correspondence to Goodarz Ahmadi, Department of Mechanical and Aeronautical Engineering, Clarkson University, Potsdam, NY 13699-5725, USA. E-mail: ahmadi@clarkson.edu

INTRODUCTION

Particle detachment from surfaces has been an important subject in the semiconductor and imaging industries. Recently, in the light of developing powder-based formulations, it has received increasing attention in pharmaceutical industries as one of the alternatives to replace Chlorofluorocarbon (CFC)-based formulations.

Drug delivery through inhalation has been widely used for treating a variety of pulmonary-related diseases, such as asthma, and other illnesses. In dry-powder inhalers, neat drugs or drugs (sizes between 1 and 5 microns), blended with excipient particles such as lactose, are dispersed and aerosolized. Chew and Chan [1] studied the effect of particle, air flow, and inhaler type on the dispersion of spray-dried mannitol powders into aerosols. Zanen *et al.* [2] analyzed the effect of inhalation flow on the performance of a dry-powder inhalation system. The influence of flow rate on aerosol particle-size distributions from pressurized and breath-actuated inhalers is reported by Smith *et al.* [3]. French *et al.* [4] studied the influence of formulation on emission, deaggregation, and deposition of dry powder for inhalation. Boer *et al.* [5] analyzed inhalation characteristics and their effects on drug delivery in dry-powder inhalers. Performance of dry-powder inhalers was also studied by Ganderton and Kassem [6].

Numerous studies concerning particle-detachment mechanisms from various surfaces have been reported by Mittal [7]. Extensive reviews of particle-adhesion mechanisms have been provided by Corn [8], Krupp [9], Visser [10], Tabor [11], Bowling [12], and Ranade [13]. Accordingly, the van der Waals force makes the major contribution to the particle-adhesion force on a surface under dry conditions. The effect of contact deformation on adhesion was first considered by Derjaguin [14]. Johnson, et al. [15] used the surface energy and surface deformation effects to develop an improved contact model called the JKR theory. According to this model, at the moment of separation, the contact area does not disappear entirely; instead, a finite contact area exists.

Otsuka *et al.* [16] measured the adhesive force between particles of powdered organic materials and a glass substrate by the impact-separation method. Podczeck *et al.* [17, 18] studied the influence of the humidity of air on the auto-adhesion force between pharmaceutical powder particles. Thornton [19] and Thornton *et al.* [20] studied the inter-particle sliding in the presence of adhesion, and performed numerical simulations of agglomerate attrition and fracture. Analyses of agglomerate strength were provided by Kendall [21].

Extensive reviews on particle-removal processes from surfaces were provided by Healy [22], Sehmel [23], Nicholson [24], and Smith *et al.*

[25]. Braaten *et al.* [26] performed an experimental study of particle re-entrainment in turbulent flow. They concluded that ejection-sweep events and macrosweep flow patterns near a wall strongly affect the particle-resuspension process. However, based on their flow visualization experiments, Yung *et al.* [27] reported that the bursting phenomenon has a small effect on entrainment of particles within the viscous sublayer.

A sublayer model for particle resuspension and deposition in turbulent flows was proposed by Cleaver and Yates [28–30]. A dynamic model for the long-term resuspension of small particles from smooth and rough surfaces in turbulent flow was developed by Reeks *et al.* [31] and Reeks and Hall [32]. A kinetic model for particle resuspension was proposed by Wen and Kasper [33] and compared with the data from industrial high-purity gas systems and with controlled experiments using latex particles of 0.4–1 μm. Soltani and Ahmadi [34, 35] studied the particle removal mechanisms from smooth and rough walls subject to substrate accelerations. Soltani and Ahmadi [36, 37] developed a flow structure–based model for turbulent resuspension and included the effect of turbulence burst. Zhang and Ahmadi [38] studied the removal and resuspension of particles in turbulent channel flows using a direct numerical-simulation approach.

Using the low-Reynolds-number hydrodynamic interactions, the drag force acting on conglomerates of spheres was studied by Durlofsky *et al.* [39], Bossis and Brady [40], Ladd [41–43], Hassonjee *et al.* [44], and Cichocki *et al.* [45]. Cichocki and Hinsen [46] provided the Stokes drag coefficients for conglomerates of between 2 and 167 spheres from the numerical calculations of hydrodynamic interactions. Kasper [47] measured the viscous drag force on cylinders and chains of spheres. Endo *et al.* [48] studied the dispersion of aggregates of fine powder by acceleration in an air stream.

In this study, the FLUENT^{TM} [49] code was used to evaluate the drag force on particle pairs. Based on the simulation results, empirical equations for predicting the drag forces acting on particle pairs attached on a plane surface were presented. The rolling and sliding detachment mechanisms were analyzed and the critical conditions for the particle-pair removal from the surface were evaluated.

FORMULATION

Drag Force

For studying the removal or breakup of a particle pair that is attached to a surface, knowledge of the hydrodynamic drag forces acting on each particle is necessary. Unfortunately, the hydrodynamic forces

acting on a particle pair resting on a surface at finite Reynolds numbers are not known. In this study, we used the computational fluid dynamics code, FLUENT^{TM} [49], to evaluate the drag force and to simulate the flow field around the two attached spherical particles that are in contact with a plane subject to a shear flow. For a range of shear rates and different sphere radii, the flow fields are simulated and the corresponding drag forces acting on each sphere are evaluated. The resulting drag forces are used to develop a new empirical equation for the drag force acting on different sized particles in various flow configurations as a function of particle Reynolds number.

Drag Force on a Single Sphere

For a stationary spherical particle in the free shear flows away from a wall, the modified Stokes drag force is given as

$$F_{\mathrm{s}} = \frac{3\pi\mu d C_N}{C_{\mathrm{c}}} u. \tag{1}$$

O'Neill [50] corrected the drag force for a sphere attached to a surface. Accordingly,

$$F_{\mathrm{o}} = \frac{3\pi f \mu d C_N}{C_{\mathrm{c}}} u. \tag{2}$$

In Equations. (1) and (2), u is fluid velocity at the centroid of the sphere, d is the sphere diameter, μ is the fluid viscosity, f (=1.7009) is a correction factor for the wall effect given by O'Neill [50], and C_c is the Cunningham correction factor given by

$$C_{\mathrm{c}} = 1 + \frac{2\lambda}{d}[1.257 + 0.4\exp(-1.1d/2\lambda)]. \tag{3}$$

In Equation (3), λ is the mean free path of the gas ($\lambda = 0.07\,\mu$m for air is used in this study). For standard Stokes drag with $\mathrm{Re}_p << 1$, $C_N = 1$ in Equations (1) and (2). For high-Reynolds-number flows, C_N is an empirical nonlinear drag correction factor given by

$$C_N = 1 + 0.15\,\mathrm{Re}_p^{0.687}, \tag{4}$$

which is used to account for the fluid inertial effects. Here Re_{p} is the particle Reynolds number defined as

$$Re_{\mathrm{p}} = \frac{ud}{\nu}, \tag{5}$$

where ν is the fluid kinematic viscosity.

Note that in Equations (1), (2), and (5), the particle is assumed to be stationary, and when the particle is moving in the flow, the particle-fluid slip-velocity, $(u^f - u^p)$ replaces the fluid velocity, u, in these equations.

Flow Model and Boundary Conditions

Because the Reynolds numbers are generally low, the viscous flow model of FLUENT^{TM} is used in the analysis. The no-slip boundary conditions on the surface of the particle pair and the wall are assumed. The inlet and the upper surface velocity conditions were selected so that a constant-shear-rate condition is imposed. The physical properties of air were also used in the analysis.

Drag Force on Two Attached Spheres

As noted before, the drag force acting on two spheres in contact (at nonzero Reynolds number) is not known. Here computer simulations are used to evaluate the drag force for two spheres for a range of flow conditions with use of the FLUENT^{TM} code.

To verify the accuracy of the simulation results, the case of a single spherical particle attached to a plane is first analyzed, and the results are compared with O'Neill's drag force. Figure 1 compares the simulated drag force with the prediction of Equation (2), for a range of shear rates, γ, for particles with diameters of 3 and 50 μm respectively. It is observed that the simulation results are in good agreement with values predicted by the O'Neill drag force. The amount of error is less than 3% for small shear rates and is about 15% at shear rate of 10^5 s^{-1}. The main reason for the discrepancy is the deviation of flow regime from the creeping flow assumption used in the derivation of the O'Neill drag force. Clearly, as the shear rate and particle size increase, the inertial effects that are neglected in the creeping flow assumption become more important.

A series of simulations are also performed for the cases of two identical particles attached together and resting on a plane surface. The schematic of two attached particles on a surface is shown in Figure 2. Here sphere 1 denotes the particle on the top and 2 denotes the particle at the bottom, which is also in contact with the surface. The case treated in this study is when the two particles are vertically aligned. In practice, however, the upper sphere could be attached to the lower sphere at different angles. The present study, therefore, provides for a limiting condition.

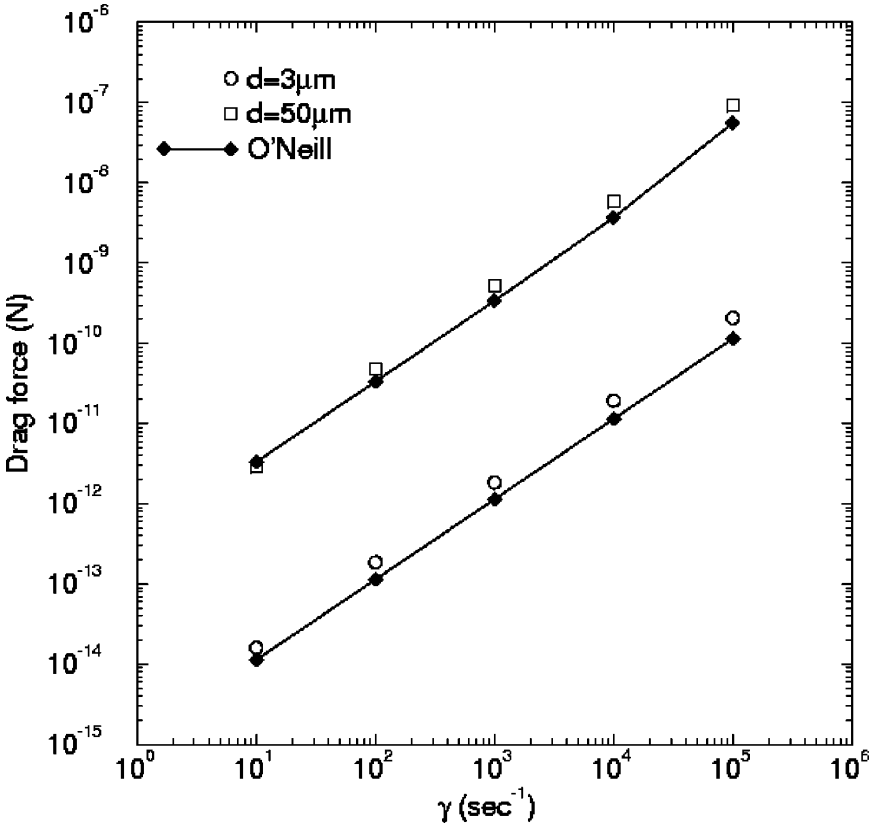

FIGURE 1 Comparison of simulated drag forces with the O'Neill equation for drag force for a sphere attached on a plane surface.

Figure 3 shows the computational grid generated by the GAMBIT™ code (see FLUENT™ manual [49]). Here 203,347 cells were used to describe the flow field around the two touching spheres. The grid is rather refined near the spheres and become coarser far from the spheres. The computational domain was a channel with a stationary lower wall and with an upper wall that is moving with a constant velocity to maintain a constant shear rate. The length of the channel was about 12 times the particle diameter and the height and the width of the domain were 6 times the diameter of the particles. Grid independence of solution was also tested for certain high shearing rates, where the grid size was doubled several times, until it was found that the effects of doubling the grid on the flow field and particularly on the drag force were negligible.

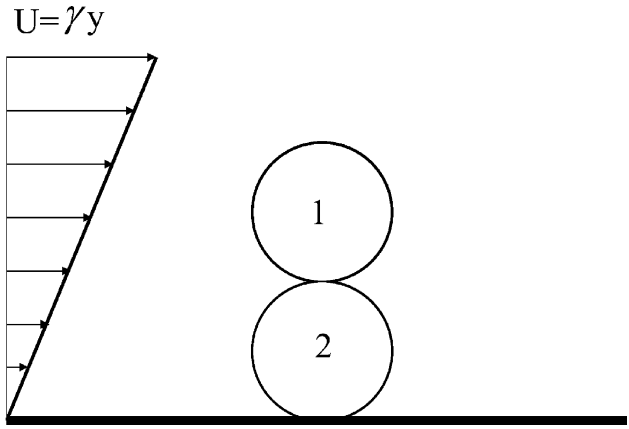

FIGURE 2 Schematic of two attached particles in touch with a plane surface in a simple shear flow.

For a shear rate of $1000\,s^{-1}$ and a particle pair with a diameter of $3\,\mu m$, Figure 4a shows the pressure contours across a plane along the flow direction that passes through the particle centroids. The high pressure in the upwind face and the lower pressure region behind the particle are clearly seen from this figure. The contour plots of the velocity field on a plane crossing the particle centroids are shown in Figure 4b. This figure shows distortion of linear shear flow field near the particle pairs.

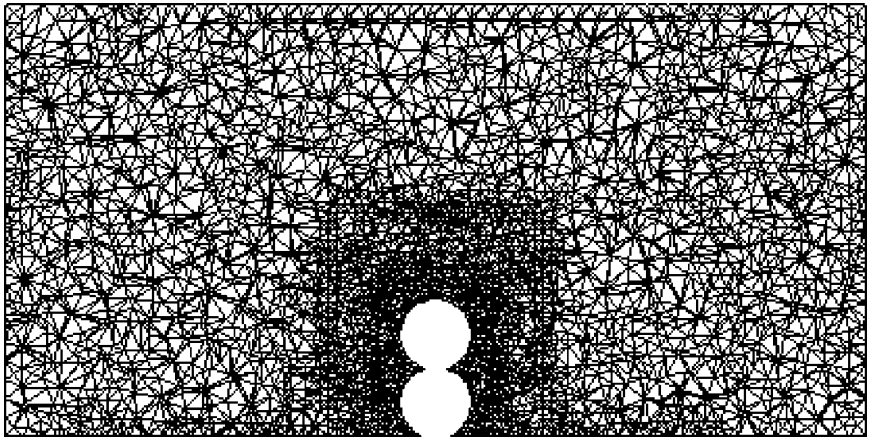

FIGURE 3 Computational grid for two attached particles on a plane surface.

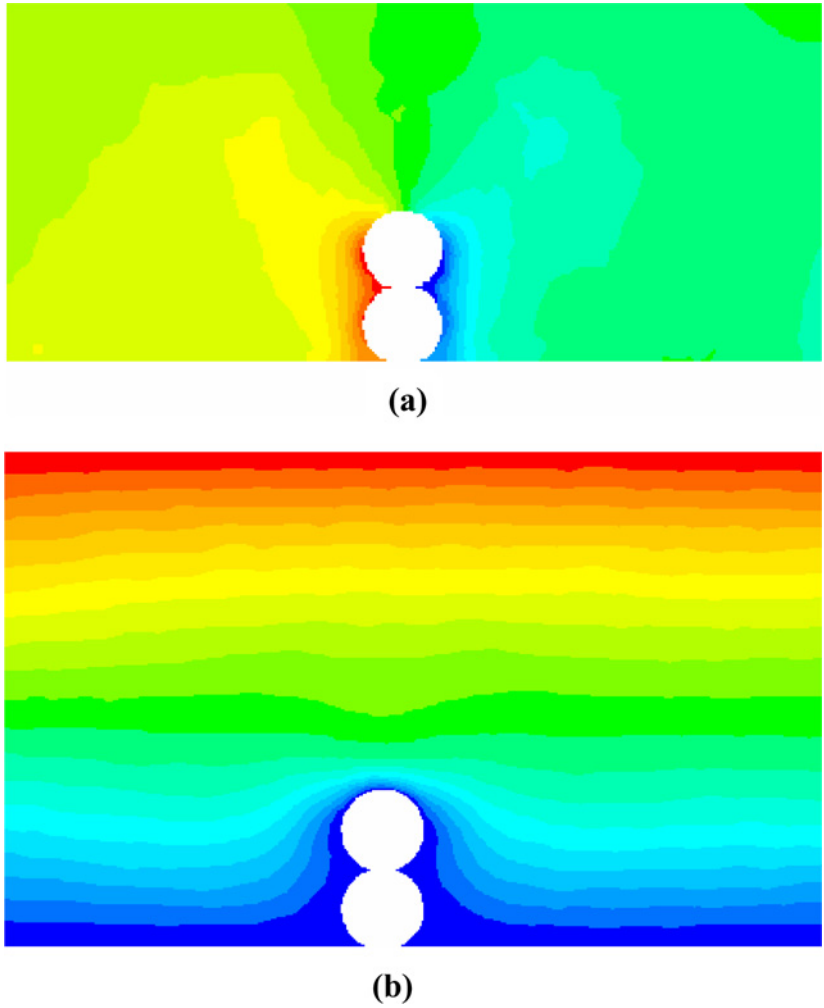

FIGURE 4 Contour plots of flow properties across a plane along the flow direction that passes through the particle centroids: (a) pressure counters; (b) velocity magnitude counters.

The computational results were used to evaluate the drag force acting on each sphere and the results are shown in Figure 5. Here doublets of equal-size spheres with diameters of 3, 25, and 50 μm are studied. For each size particle, there are two identical shape symbols in this figure; the hollow ones correspond to the particle on the top and the solid symbol corresponds to the particle on the bottom, which is in

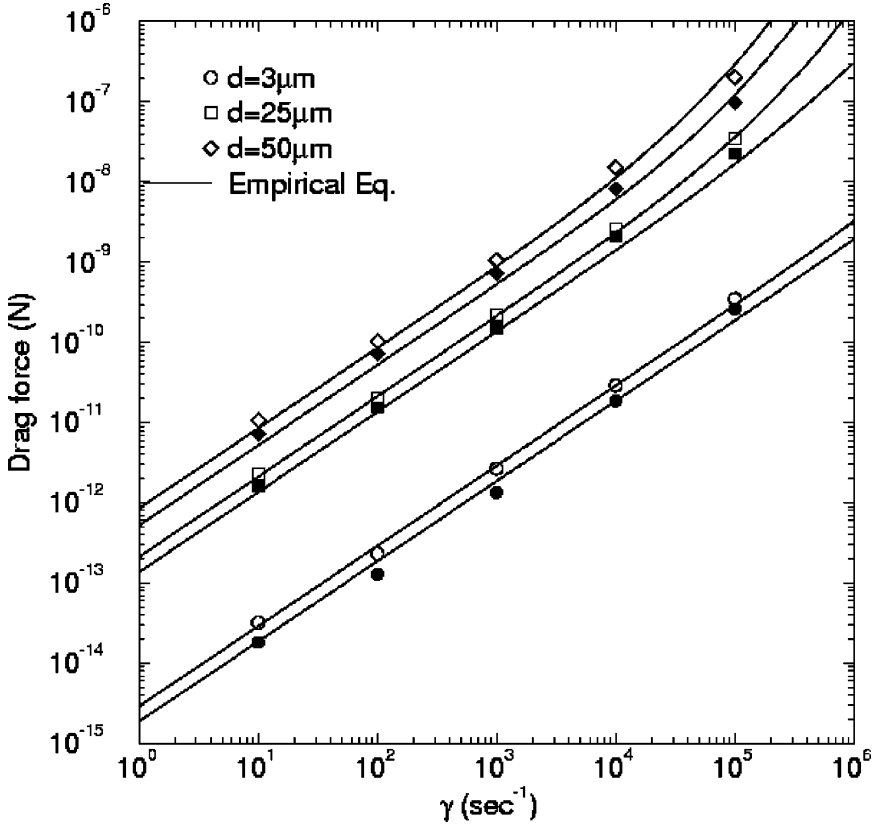

FIGURE 5 Comparison of simulated drag forces with the empirical equations.

contact with the surface. It is observed that the drag force increases rapidly as shear rate increases. The hollow symbols are higher compared to the solid ones because the sphere on the top is exposed to higher velocity and experiences higher drag force. The data for the simulated drag forces on a single sphere and pairs of equal-size spheres are listed in Tables A1 and A2 in Appendix A.

Based on the simulation results for the drag forces, we developed two empirical equations for predicting the drag force that acts on each particle in a vertically aligned configuration of a pair of equal-size spheres for a range of Reynolds numbers. These are

$$F_{d1} = (1.448 + 0.0266\,Re_p)F_s, \quad \text{for sphere 1 (top sphere)}, \qquad (6)$$

$$F_{d2} = (1.569 + 0.0751\,Re_p)F_o, \quad \text{for sphere 2 (lower sphere)}, \qquad (7)$$

where F_s and F_o are drag forces given by Equations (1) and (2). That is, for the particle on the top, we modified the Stokes drag by the correction factor shown in Equation (6). Also, for the lower particle, which is in contact with the wall, the corrected O'Neill drag is given by Equation (7).

The predictions of empirical equations given by (6) and (7) are plotted in Figure 5 for comparison with the simulation results. It is observed that the empirical equation predictions are in good agreement with the simulation results. The amount of error is less than 5% for small shear rates and is about 15% at shear rate of $10^5\,s^{-1}$. Thus, Equations (6) and (7) are used for evaluating the drag force acting on two attached identical particles in contact with a surface. It is also of interest to note that for the creeping flow condition, as Re_p becomes small, the upper sphere experiences 45% additional drag when compared with the Stokes drag. Similarly, the lower sphere, which is contact with the surface, experiences 57% more drag when compared with the O'Neill drag force.

For drag force acting on a pair of unequal spheres we used the following empirical expressions:

$$F_{d1} = [1 - (0.235 - 0.0248\,Re_{p1})(1 - e^{-d_2/d_1})]F_{od1}, \quad \text{for sphere 1 (top sphere)}, \tag{8}$$

$$F_{d2} = [1 + (0.9 + 0.12\,Re_{p2})(1 - e^{-d_1/d_2})]F_{od2}, \quad \text{for sphere 2 (lower sphere)}, \tag{9}$$

where F_o is the drag force given by Equation (2), and subscripts 1 and 2, respectively, refer to the top and the bottom particles. When the particles are of equal sizes, Equations (8) and (9) reduce to Equations (6) and (7). For the limit that $d_1 << d_2$, the drag on the lower sphere becomes the O'Neill drag for a sphere attached to a surface. The smaller sphere on the top experiences a drag somewhat smaller than O'Neill drag and larger than Stokes drag. For the limit that $d_2 << d_1$, the drag on the upper sphere reduces to O'Neill's drag for a sphere attached to a surface. The smaller sphere on the bottom experiences a drag is larger than O'Neill drag by more than 90%.

Adhesion Force

Johnson, Kendall, and Roberts [15] developed a particle-adhesion model that included the effect of elastic surface deformation. The Johnson, Kendall, and Roberts (JKR) model was used in this study for evaluating the adhesion force between particles, between the

particle and the substrate, and for their detachment. According to the JKR theory, when two particles adhere together, a finite contact area forms, and in the absence of external forces, the radius of the contact circle, a_0, is given as

$$a_0^3 = \frac{6\pi W_A R^2}{K}, \tag{10}$$

where

$$K = \frac{4}{3}\left[\frac{(1-\nu_1^2)}{E_1} + \frac{(1-\nu_2^2)}{E_2}\right]^{-1} \tag{11}$$

is the composite Young modulus. Here, R is the effective radius, given by

$$R = \frac{r_1 r_2}{r_1 + r_2}, \tag{12}$$

where r_1 and r_2 are the radii of the particles. Equation (12) becomes $R = r_2$ (the radius of the lower particle) while evaluating the adhesion between the lower particle and the substrate. In Equation (10), W_A is the thermodynamic work of adhesion, and ν_i and E_i are, respectively, the Poisson ratio and the Young modulus of material i (i =1 or 2).

According to the JKR model, the pull-off force F_p, for removing a particle from a surface or detaching two particles from each other, is given by

$$F_p = \frac{3}{2}\pi W_A R. \tag{13}$$

When two different materials with thermodynamic work of adhesion of W_{A1} and W_{A2} are in contact, the combined effective surface energy, W_A, may be evaluated approximately using

$$W_A = \sqrt{W_{A1} W_{A2}}. \tag{14}$$

At the moment of separation, the JKR theory predicts that a finite contact area exists with its radius given as

$$a = a_0/4^{1/3}. \tag{15}$$

It should be emphasized that the JKR model is suitable for the adhesion of particles to a surface for relatively soft materials and when no plastic deformation occurs. For very hard materials and when plastic deformation occurs, other adhesion models (Derjaguin [14], Muller *et al.* [51], and Maugis and Pollock [52]) need to be used.

Detachment Model

Particles may be detached by rolling or sliding mechanisms. Figure 6 shows the geometric features of two attached spherical particles on a plane surface. When the drag force is greater than the frictional resistance, the particle will be removed by the sliding detachment mechanism. The criteria for the sliding detachment mechanism are given as

$$F_{\mathrm{d1}} \geq k_1 F_{\mathrm{p1}}, \quad \text{for detachment of upper particle (sphere 1)}, \tag{16}$$

$$F_{\mathrm{d1}} + F_{\mathrm{d2}} \geq k_2 F_{\mathrm{p2}}, \quad \text{for detachment of particle pair}, \tag{17}$$

where F_{d1} and F_{d2}, respectively, are the drag forces acting on the upper and lower spheres, F_{p1} is the adhesion pull-off force between particles and F_{p2} is the adhesion pull-off force between the lower particle and the surface, and k_1 and k_2 are the frictional coefficients between the particles and between the lower sphere and the wall. Note that Equation (17) assumes that inequality (16) does not hold and the particle pair remains attached. If the upper particle is detached, then the condition for sliding detachment of the lower particle is simply $F_{\mathrm{d2}} \geq k_2 F_{\mathrm{p2}}$

When the moments induced by the drag forces overcome the resistance moments of the adhesion pull-off forces with respect to points O_1 and O_2, the particles will be detached from the surface by the rolling mechanism. The rolling detachment criteria then are

$$F_{\mathrm{d1}}(r_1 - \alpha_{01}) \geq F_{\mathrm{p1}} a_1, \quad \text{for detachment of upper particle (sphere 1)}, \tag{18}$$

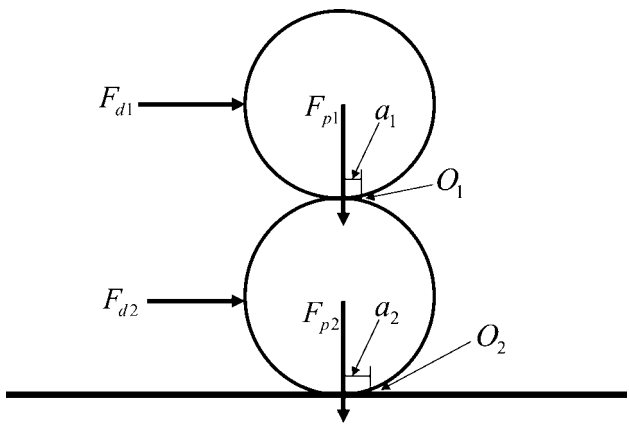

FIGURE 6 Geometric features of two attached spherical particles on a plane surface.

$$F_{d1}(r_1 + 2r_2 - \alpha_{01} - \alpha_{02}) + F_{d2}(r_2 - \alpha_{02}) \geq F_{p2}a_2, \quad \text{for detachment of particle pair.} \tag{19}$$

Here a_1 and a_2 are, respectively, the contact radius of the top and bottom spheres at the moment of separation given by Equation (15). In Equations (18) and (19),

$$\alpha_{01} = r_1 - \sqrt{r_1^2 - a_1^2}, \tag{20}$$

$$\alpha_{02} = r_2 - \sqrt{r_2^2 - a_2^2}, \tag{21}$$

are, respectively, the relative approaches between the two spheres and between the lower sphere and the wall. Again, Equation (19) assumes that the particle pair remains attached. Equations (16)–(19) are used for evaluating the critical shear rate for breakup of the top particle from the bottom particle, and for detachment of the particle pair from the surface.

Dry-Powder Inhaler

Dry-powder inhalers are used extensively for inhalation pharmaceutical drug delivery. The dispersion chamber of the inhaler is normally made of polycarbonate. Micronized drug particles are blended with the lactose carrier particles, which have an average diameter of approximately 150 μm. The material properties of lactose are listed in Table 1 (Boerefijn *et al.* [53]). In this table, the friction coefficients listed are estimated based on similar materials. In the earlier work of Soltani and Ahmadi [37, 54], it was shown that the presence of fine surface roughness reduces the magnitude of pull-off force. As a first approximation, here to account for the particle surface roughness, the thermodynamic work of adhesion for a rough lactose particle is reduced by a factor of ten to $W_A = 0.05\,J/m^2$ as shown in Table 1. This corresponds to a surface bump radius of 0.3 μm and a roughness variance of 3 nm in the model of Soltani and Ahmadi [37, 54]. For smooth lactose particle attached on a polycarbonate surface, the combined surface energy is given by Equation (14) as $W_A = 0.0727\,J/m^2$. For a rough lactose particle attached on a polycarbonate surface, the combined surface energy is $W_A = 0.023\,J/m^2$.

Pull-Off Force

For a range of sizes of two identical lactose particles, Figure 7 shows the pull-off force required to remove the upper sphere (sphere 1) from the lower particle and the pull-off force needed to detach the lower particle

TABLE 1 Material Properties

Material	E Gpa	W_A (J/m^2)	ρ (10^3 kg/m^3)	ν_i	k	Y Gpa
Smooth powder (Lactose–Lactose)	3.2	0.5	1.550	0.3	0.35	0.21
Rough powder (Lactose–Lactose)	3.2	0.05	1.550	0.3	0.35	0.21
Substrate (Polycarbonate–Polycarbonate)	2.4	0.0105	11.57	0.38	0.35	—
Impeller (Delrin–Delrin)	3.1	0.0105	—	0.35	0.35	0.069

(sphere 2) from the polycarbonate substrate. Figure 7 shows that for both smooth and rough lactose particles, the pull-off force for removing the upper particle is larger than that for removing the particle pair from the

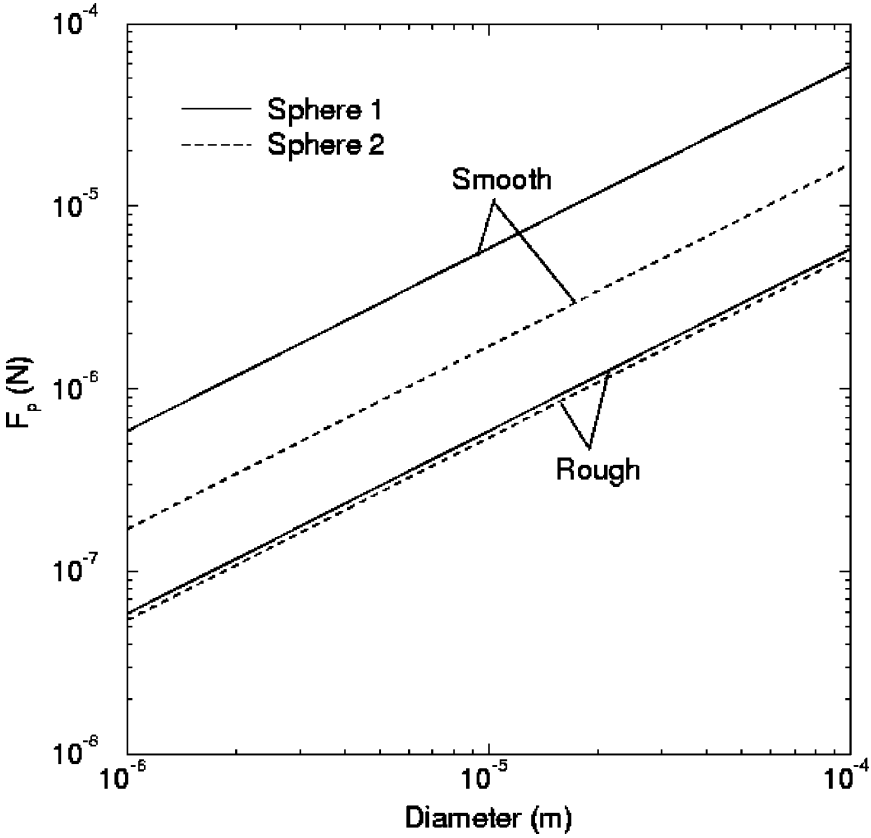

FIGURE 7 Variations of the pull-off force with lactose particle diameter for pairs of identical spheres.

surface. This is because the surface energy is higher between two lactose particles than that between the bottom particle and the surface. It is also observed that the pull-off force increases as the particle size increases and the surface roughness reduces the pull-off forces.

Variations of the contact radius at the moment of separation between lactose particles and at the particle–surface interface for a pair of identical lactose particles are shown in Figure 8. Here, a polycarbonate substrate is assumed. This figure shows that the contact radius increases with the particle size. For smooth lactose particles, the contact radius between the particles is larger than that between the lactose particle and the polycarbonate substrate because of the higher surface energy. For the case of rough lactose particles, however, Figure 8 shows that the contact radius between the lower

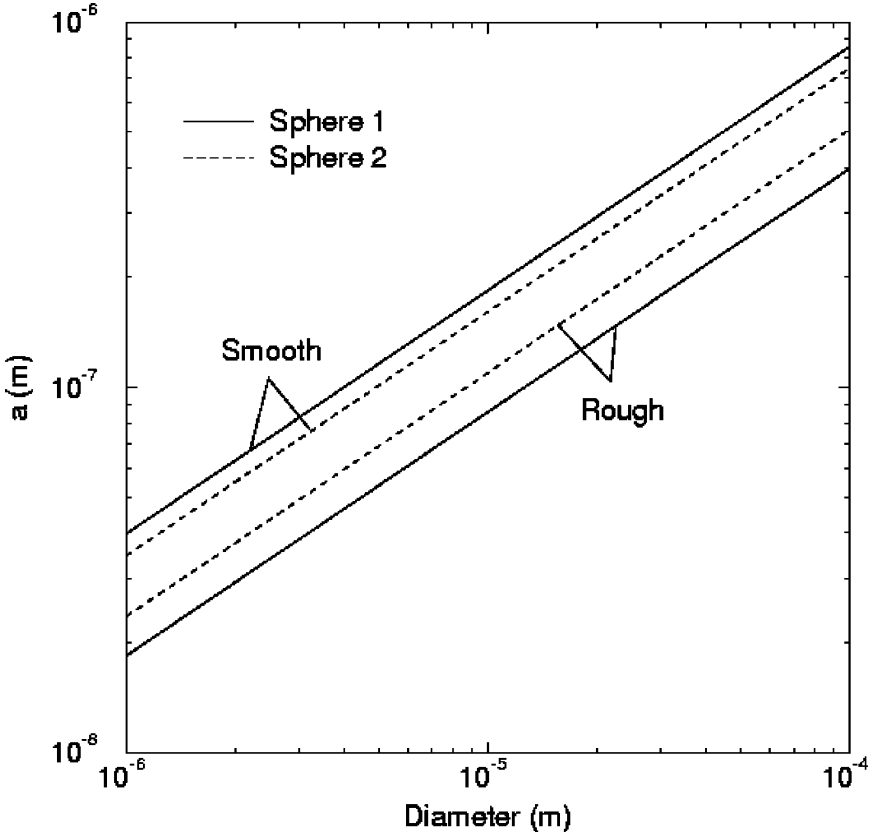

FIGURE 8 Variations of the contact radius with particle diameter.

particle and the surface is larger than that between the particles. This is because the surface energies are comparable and the effect of particle radius for sphere–plane contact is larger than that for two spheres. This figure also shows that the presence of surface roughness reduces the contact area.

RESULTS AND DISCUSSION

There are two possibilities for detachment of two attached (and vertically aligned) particles in contact with a surface. One is that the upper particle is detached and the lower one remains attached to the surface. In this case, the contact between the spheres fails. The other is that the two particles remain attached but are removed together from the surface. Here the contact between the bottom sphere and the wall fails. The critical shear rates for detachment of pairs of lactose spheres from a polycarbonate substrate by these different removal mechanisms are evaluated. Clearly, if the critical shear rate for removal of the upper particle is lower than that for removal of both particles, the upper particle will be removed and the bottom particle remains attached to the surface. Otherwise, both particles will be removed but remain attached together.

For identical smooth lactose particles, Figure 9a shows the critical shear rates for removal of the upper lactose particle from the lower one and for detaching both lactose particles from the polycarbonate surface. The critical shear rate for both sliding and rolling detachment mechanisms are also shown in this figure. The critical shear rates for particle removal by the sliding mechanism are much higher than those by rolling mechanism. Therefore, the rolling detachment is the dominant mechanism for spherical particle removal. Figure 9a shows that the critical shear rate decreases as particle size increases. That is, large particles are more easily removed when compared with small particles. Figure 9a also shows that for both sliding and rolling detachment mechanisms, the critical shear rate for upper particle removal is higher than that for detaching both particles. This indicates that for two identical smooth lactose particles attached together on a polycarbonate surface, particle pairs will be removed. This is because the adhesion force between particles is much larger than that between the lower particle and the surface. Thus, both particles will be removed together.

The corresponding critical shear rates for identical rough lactose particle detachment are shown in Figure 9b. This figure shows that the critical shear rate for the rolling detachment mechanism is lower than that for the sliding detachment. For identical rough lactose particles, particle pairs will be removed at lower shear rates. Comparing

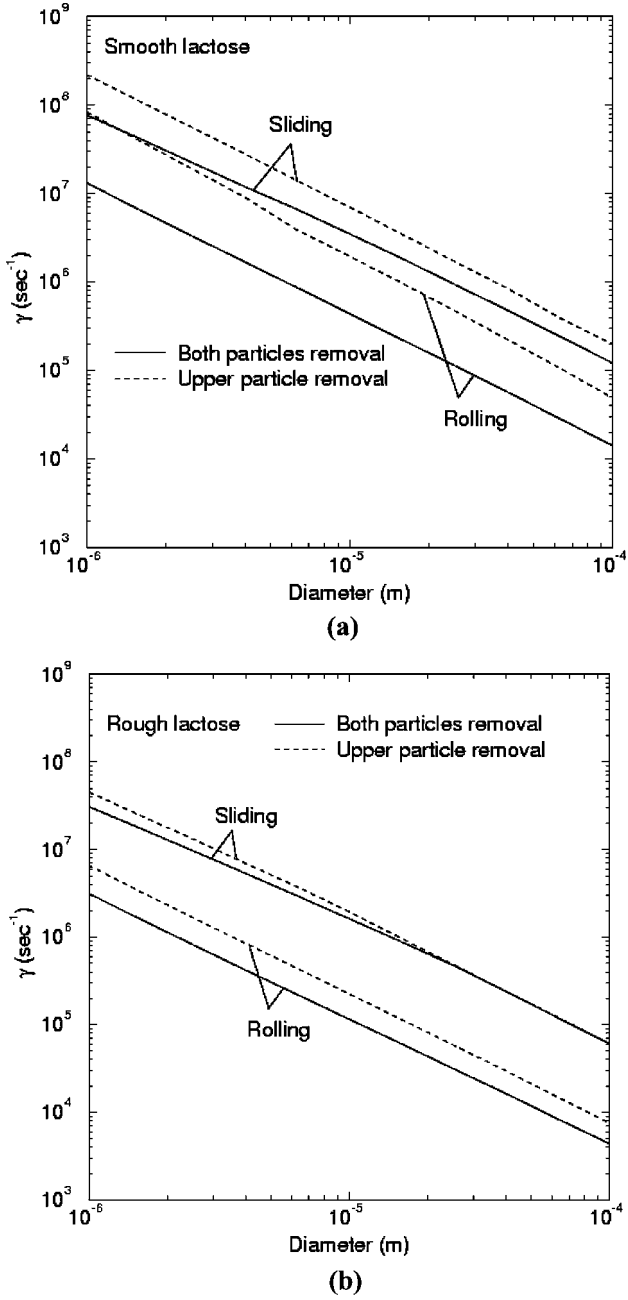

FIGURE 9 Variations of the critical shear rate for removal of identical particle pairs: (a) smooth lactose particle pairs; (b) rough lactose particle pairs.

Figures 9a and 9b shows that the critical shear rate decreases significantly for removal of rough particles.

It should be emphasized that at high shear rates, when the flow becomes turbulent, the effect of turbulence burst on particle removal becomes important (Soltani and Ahmadi, [36]). To evaluate the critical turbulent flow properties for particle removal based on the estimated critical shear rate, the effect of turbulence burst should be included.

For different-size smooth lactose particles, Figure 10a shows the critical shear rates for removal of the upper particle, as well as both particles from the surface versus diameter ratio d_2/d_1. In this figure, the upper particle is assumed to have a fixed diameter at $d_1 = 3\,\mu m$. The critical shear rate for both sliding and rolling detachment mechanisms are also shown in this figure. The critical shear rates for particle removal by the sliding mechanism are much higher than those by the rolling mechanism. Figure 10a shows that the critical shear rate for removal of the attached particle from the surface by the rolling mechanism is the lowest. Thus, the attached lactose particles will be removed by the rolling detachment mechanism from the polycarbonate substrate. Figure 10a also shows that the critical shear rate reaches a peak value at about $d_2/d_1 \approx 1$. This indicates that particle pairs can be more easily detached when their size differences become large. In particular, for the dry powder inhaler, $d_2/d_1 = 50$ and the critical shear rate for removal of a $150\,\mu m$ carrier and a $3\,\mu m$ drug particle from the surface is $9500\,s^{-1}$

Figure 10b shows the critical shear rate for removal of rough lactose particles by both sliding and rolling detachment mechanisms. The critical shear rate for removal by the sliding detachment is much higher than that for the rolling detachment. For rough lactose particles in this figure, the particle pairs will be removed by the rolling mechanism. For $d_1 = 3\,\mu m$ and $d_2 = 150\,\mu m$, the critical shear rate for removal of a particle pair is $2600\,s^{-1}$. Thus, particles with fine roughness can be more easily removed from the surface. The critical shear rate for removing a 3-μm drug particle from a 150-μm carrier particle that is resting on the wall is about $1 \times 10^5\,s^{-1}$

Figure 11a shows the critical shear rates when the upper particle diameter is fixed at $d_1 = 150\,\mu m$ and the lower particle diameter is smaller than the upper one. Here the rolling detachments of both smooth and rough lactose particles are considered. It is observed that for both smooth and rough lactose particles, the particle pairs will be removed. The critical shear rate increases as the lower particle size increases. That is, as d_2/d_1 decreases, the particle can be removed more easily. Specifically, for $d_1 = 150\,\mu m$ and $d_2 = 3\,\mu m$, the critical shear rate is $1800\,s^{-1}$ for smooth lactose particles and $15\,s^{-1}$ for rough lactose particles. The

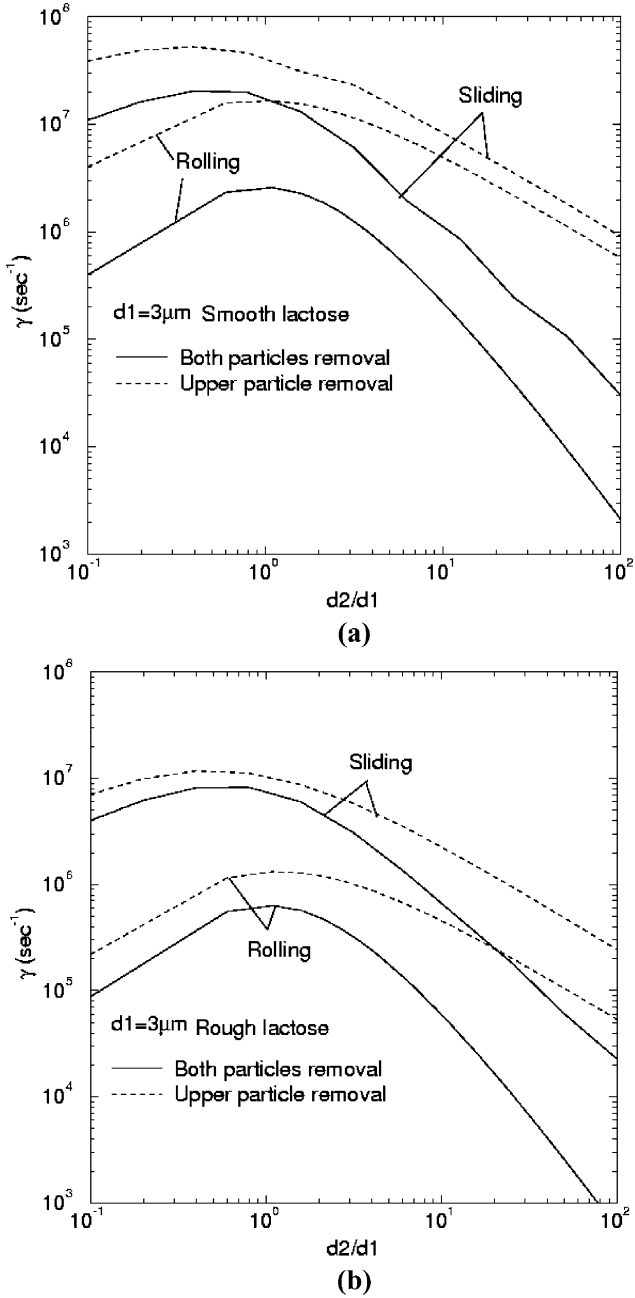

FIGURE 10 Variations of the critical shear rate for breakup of pairs of different size particles: (a) smooth lactose particle pairs; (b) rough lactose particle pairs.

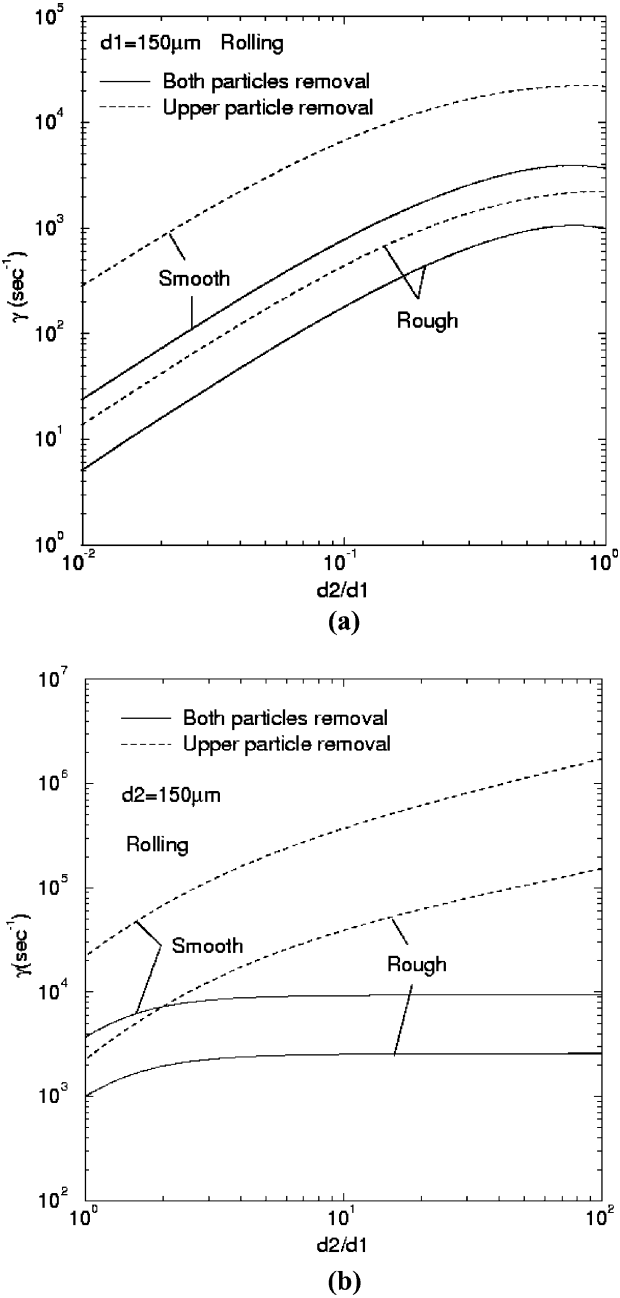

FIGURE 11 Variations of the critical shear rate for removal of lactose particle pairs: (a) $d_1 = 150$ μm; (b) $d_2 = 150$ μm.

TABLE 2 Critical Shear Rate for Particle Removal

	Smooth lactose	Rough lactose
$d_1 = 3\,\mu m$	9500	2600
$d_2 = 150\,\mu m$	both particles removed	both particles removed
$d_1 = 150\,\mu m$	1800	15
$d_2 = 3\,\mu m$	both particles removed	both particles removed

critical shear rates for removal of an attached 3–150 μm particle pair are listed in Table 2. This table shows that the critical shear rate is lowest for a pair with upper large and lower small particles.

The critical shear rate for the case when the lower particle is larger than the upper one is shown in Figure 11b. Here, the lower sphere is assumed to be a carrier particle with a diameter of $d_2 = 150\,\mu m$ and a range of sizes for the upper drug particle (smaller than that of carrier particle) is considered. Figure 11b shows that for both smooth and rough lactose particles, particle pairs will be removed. For particle-pair removal, the critical shear rate for removal changes slightly when $d2/d1 > 2$. This result is as expected because the drag force acting on the large 150-μm carrier particle is not affected by the presence of a small drug particle.

CONCLUSIONS

In this study, the critical conditions for vertically aligned particle-pair removal from a surface were evaluated and the rolling and sliding detachment mechanisms were analyzed. In the process, semi-empirical equations for drag on a pair of attached spheres were developed. On the basis of the results presented, the following conclusions are drawn:

- The rolling detachment is the dominant mechanism for breakup of particle agglomerates from a plane surface.
- Rough lactose particle pairs can be more easily removed compared with smooth lactose particle pairs.
- For the range of particle sizes used in the simulations, the particle pairs are removed from the wall but remain attached.
- It is easier for a pair particle with the large particle on the top to be removed from the wall when compared with a pair with the large particle in contact with the wall.

In the present study the limiting case of aligned particles was studied. Analysis of the more general case where the particles are not vertically aligned is left for a future study.

REFERENCES

[1] Chew, N. Y. K. and Chan, H.-K., Influence of particle size, air flow, and inhaler device on the dispersion of mannitol powders as aerosols, *Pharmaceutical Research* **16**, 1098–1103 (1999).
[2] Zanen, P., Van Spiegel, P. I., Van der Kolk, H., Tushuizen, E., and Enthoven, R., The effect of the inhalation flow on the performance of a dry powder inhalation system, *Int. J. Pharm.* **81**, 199–203 (1992).
[3] Smith, K. J., Chan, H.-K. and Brown, K. F., Influence of flow rate on aerosol particle size distributions from pressurized and breath-actuated inhalers, *J. Aerosol Med.* **11**, 231–245 (1998).
[4] French, D. L., Edwards, D. A., and Niven, R. W., The influence of formulation on emission, deaggregation and deposition of dry powders for inhalation, *J. Aerosol Sci.* **27**, 769–783 (1996).
[5] De Boer, A. H., Gjaltema, D., and Hagedoorn, P., Inhalation characteristics and their effects on in vitro drug delivery from dry powder inhalers, Part 2: Effect of peak flow rate (PIFR) and inspiration time on the in vitro drug release from three different types of commercial dry powder inhalers, *Int. J. Pharm.* **138**, 45–46 (1996).
[6] Ganderton, D. and Kassem, N. M., Dry powder inhalers, in *Advances in Pharmaceutical Sciences,* D. Ganderton and T. Jones (Eds.) (Academic Press, London, 1992), pp. 165–191.
[7] Mittal, K. L. (Ed.) *Particles on Surface: Detection, Adhesion and Removal*, Vol. 3 (Plenum Press, New York, 1991).
[8] Corn, M., in *Aerosol Science*, C. N. Davies (Ed.) (Academic Press, New York, 1966), p. 359.
[9] Krupp, H., Particle adhesion: Theory and experiment, *Adv. Colloid Interface. Science* **1**, 111–140 (1967).
[10] Visser, J., Adhesion of colloidal particles, *Surface and Colloid Science*, **8**, 3–84 (1976).
[11] Tabor, D., *Fluid Dynamics of Multiphase System* (Blaisdell Pub. Co., New York, 1977).
[12] Bowling, R. A., An analysis of particle adhesion on semiconductor surfaces, *J. Electrochem. Soc. Solid State Science Technol.* **132**, 2208–2219 (1985).
[13] Ranade, M. B., Adhesion and removal of fine particles on surfaces, *J. Aerosol Sci. Technol.* **7**, 161–176 (1987).
[14] Derjaguin, B. V. Untersuchungen über die Reibung und adhäsion, IV. *Koll. Z.* **69**, 155–164 (1934).
[15] Johnson, K. L., Kendall, K., and Roberts, A. D., Surface energy and contact of elastic solids, *Proc. R. Soc. London* **324**, 301–313 (1971).
[16] Otsuka, A., Kida, K., Danjo, K., and Sunada, H., Measurement of the adhesive force between particles of powdered organic materials and a glass substrate by means of the impact separation method, I. Effect of temperature, *Chem. Pharm. Bull.* **31**, 4483–4488 (1983).
[17] Podczeck, F., Newton, J. M., and James, M. B., The influence of constant and changing relative humidity of the air on the autoadhesion force between pharmaceutical powder particles, *Int. J. Pharm.* **145**, 221–229 (1996).
[18] Podczeck, F., Newton, J. M., and James, M. B., Influence of relative humidity of storage air on the adhesion and autoadhesion of micronized particles to particulate and compacted powder surfaces, *J. Colloid Interface Sci.* **187**, 484–491 (1997).
[19] Thornton, C., Interparticle sliding in the presence of adhesion, *J. Phys. D: Appl. Phys.* **24**, 1942–1946 (1991).

[20] Thornton, C., Kafui, K. D., Ciomocos, M. T., and Adams, M. J., Numerical simulation of agglomerate attrition and fracture, *Proc. 1st Eur. Congr. Chem. Eng.* **2**, 919–922 (1997).
[21] Kendall, K., Agglomerate strength, *Powder Metallurgy* **31**, 28–31 (1988).
[22] Healy, J. W., *A review of resuspension models. In transuranics in natural environments*, M. G. White and P. B., Dunaway, (Eds.) (USERDA, Las Vegas, 1977), pp. 211–222.
[23] Sehmel, G. A., Particle resuspension: A review, *Environ. Int.* **4**, 107–127 (1980).
[24] Nicholson, K. W., A review of particle resuspension, *Atmospheric Environment* **22**, 2639–2651 (1988).
[25] Smith, W. J., Whicher, F. W., and Meyer, H. R., Review and categorization of saltation, suspension and resuspension models, *Nuclear Safety* **23**, 685–699 (1982).
[26] Braaten, D. A., Paw, U. K. T., and Shaw, R. H., Coherent turbulent structures and particle detachment in boundary layer flows, *J. Aerosol Sci.* **19**, 1183–1186 (1988).
[27] Yung, B. P. K., Merry, H., and Bott, T. R., The role of turbulent bursts in particle re-entrainment in aqueous system, *Chem. Eng. Sci.* **44**, 873–882 (1989).
[28] Cleaver, J. W. and Yates, B., Mechanism of detachment of colloid particles from a flat substrate in turbulent flow, *J. Colloid Interface Sci.* **44**, 464–474 (1973).
[29] Cleaver, J. W. and Yates, B., A sublayer model for deposition of the particles from turbulent flow, *Chem. Eng. Sci.* **30**, 983–992 (1975).
[30] Cleaver, J. W. and Yates, B., The effect of re-entrainment on particle deposition, *Chem. Eng. Sci.* **31**, 147–151 (1976).
[31] Reeks, M. W., Reed, J., and Hall, D., On the resuspension of small particles by a turbulent flow, *J. Phys. D: Appl. Phys.* **21**, 574–589 (1988).
[32] Reeks, M. W. and Hall, D., Deposition and resuspension of gas borne particles in recirculating turbulent flows, *J. Fluid Eng.* **110**, 165–171 (1988).
[33] Wen, H. Y. and Kasper, G., On the kinetics of particle reentrainment from surfaces, *J. Aerosol Sci.* **20**, 483–398 (1989).
[34] Soltani, M. and Ahmadi, G., Particle removal mechanism under base acceleration, *J. Adhes.* **44**, 161–175 (1994).
[35] Soltani, M. and Ahmadi, G., Particle detachment mechanisms from rough surfaces under substrate acceleration, *J. Adhes. Sci. Technol.* **9**, 453–373 (1995).
[36] Soltani, M. and Ahmadi, G., On particle adhesion and removal mechanisms turbulent flows, *J. Adhes. Sci. Technol.* **8**, 763–785 (1994).
[37] Soltani, M. and Ahmadi, G., Particle detachment from rough surfaces in turbulent flows, *J. Adhes.* **51**, 105–123 (1995).
[38] Zhang, H. and Ahmadi, G., Aerosol particle removal and re-entrainment in turbulent channel flows: A direct numerical simulation approach, *J. Adhes.* **74**, p. 441–493 (2000).
[39] Durlofsky, L., Brady, F. J., and Bossis, G., Dynamic simulation of hydrodynamically interacting particles, *J. Fluid Mech.* **180**, 21 (1987).
[40] Bossis, G. and Brady, F. J., Dynamic simulation of sheared suspensions. I. General method, *J. Chem. Phys.* **80**, 5141 (1984).
[41] Ladd, A. J. C., Hydrodynamic interactions in a suspension of spherical particles, *J. Chem. Phys.* **88**, 5051 (1988).
[42] Ladd, A. J. C., Hydrodynamic interactions and the viscosity of suspensions of freely moving spheres, *J. Chem. Phys.* **90**, 1149 (1989).
[43] Ladd, A. J. C., Hydrodynamic transport coefficients of ransom dispersion of hard spheres, *J. Chem. Phys.* **93**, 3484 (1990).

[44] Hassonjee, Q., Ganatos, P., and Pfeffer, R., A strong-interaction theory for the motion of arbitrary three-dimensional clusters of spherical particles at low Reynolds numbers, *J. Fluid Mech.* **197**, 1 (1988).
[45] Cichocki, B., Felderhof, U. B., Hinsen, K., Wajnryb, E. and Blawzdziewicz, J., Friction and mobility of many spheres in Stokes flow, *J. Chem. Phys.* **100**, 3780 (1994).
[46] Cichocki, B. and Hinsen K., Stokes drag on conglomerates of spheres, *Phys. Fluids* **7**, 285–291 (1994).
[47] Kasper G., Measurements of viscous drag on cylinders and chains of spheres with aspect ratios between 2 and 50, *J. Aerosol Sci.* **16**, 535–556 (1985).
[48] Endo, Y., Hasebe, S., and Kousaka, Y., Dispersion of aggregates of fine powder by acceleration in an air stream and its application to the evaluation of adhesion between particles, *Powder Technology* **91**, 25–30 (1997).
[49] *FLUENT Users Guide* (FLUENT Corporation, Lebanon, NH, 1998).
[50] O'Neill, M. E, A sphere in contact with a plane wall in a slow linear shear flow, *Chem. Eng. Sci.* **23**, 1293–1298 (1968).
[51] Muller, V. M., Yu, V. S., and Derjaguin, B. V., On the influence of molecular forces on the deformation of an elastic sphere and its sticking to a rigid plane, *J. Colloid Interface Sci.* **77**, 91–101 (1980).
[52] Maugis, D. and Pollock, H. M., Surface forces, deformation and adherence at metal microcontacts, *Acta Metall.* **32**, 1323–1334 (1984).
[53] Boerefijn, R., Ning, Z., and Ghadiri, M., Disintegration of weak lactose agglomerates for inhalation applications, *Int. J. Pharm.* **172**, 199–209 (1998).
[54] Soltani, M. and Ahmadi, G., Particle detachment from rough surfaces in turbulent flows, *J. Adhes.* **51**, 105–123 (1999).

APPENDIX A

TABLE A1 Simulated Drag Force (N) on a Sphere Attached on a Surface

Shear rate γ	$d = 3\,\mu m$	$d = 50\,\mu m$
10	1.62e-14	2.89e-12
10^2	1.87e-13	4.87e-11
10^3	1.87e-12	5.23e-10
10^4	1.95e-11	5.82e-9
10^5	2.09e-10	9.21e-8

TABLE A2 Simulated Drag Force (N) on Two Equal-Size Attached Spheres on a Surface

Shear rate γ	$d_1 = 3\,\mu m$	$d_2 = 3\,\mu m$	$d_1 = 25\,\mu m$	$d_2 = 25\,\mu m$	$d_1 = 50\,\mu m$	$d_2 = 50\,\mu m$
10	3.23e-14	1.83e-14	2.23e-12	1.62e-12	1.07e-11	7.18e-12
10^2	2.32e-13	1.30e-13	2.05e-11	1.56e-11	1.03e-10	7.24e-11
10^3	2.68e-12	1.36e-12	2.24e-10	1.54e-10	1.07e-9	7.26e-10
10^4	2.93e-11	1.88e-11	2.56e-9	2.08e-9	1.53e-8	8.20e-9
10^5	3.52e-10	2.54e-10	3.53e-8	2.27e-8	2.04e-7	9.71e-8